



## STRESS–STRAIN RELATION OF CuAlNi SMA SINGLE CRYSTAL UNDER BIAXIAL LOADING—CONSTITUTIVE MODEL AND EXPERIMENTS

D.-N. FANG<sup>1</sup>, W. LU<sup>1</sup>, W.-Y. YAN<sup>1</sup>, T. INOUE<sup>2</sup> and K.-C. HWANG<sup>1†</sup>

<sup>1</sup>Failure Mechanics Laboratory, Department of Engineering Mechanics, Tsinghua University, Beijing 100084, P.R. China and <sup>2</sup>Department of Energy Conversion Science, Kyoto University, Yoshida-Honmachi, Sakyo-ku 606-8501, Kyoto, Japan

(Received 14 August 1998; accepted 22 August 1998)

**Abstract**—In the previous work of two of the authors, a generalized micromechanics constitutive model was developed to describe thermoelastic martensitic transformation. In order to verify the theory and to investigate basic properties of thermoelastic martensitic transformation in shape memory alloys (SMA), uniaxial and biaxial loading tests under different combined loads at a constant temperature were performed on cruciform specimens of a SMA CuAlNi single crystal. The crystallographic theory for martensitic transformation has been employed to calculate the orientations of martensite variants and the transformation plastic strain. Experimental data were compared with theoretical calculation by the generalized constitutive model based on micromechanics. The results show that the constitutive theory can describe the complex thermodynamic processes, such as the forward transformation, reverse transformation and reorientation happening simultaneously, and the theoretical predictions consist well with experiments. © 1998 Acta Metallurgica Inc. Published by Elsevier Science Ltd. All rights reserved.

### 1. INTRODUCTION

Martensitic transformation can be induced by the application of stress as well as by change in temperature. When the shape and volume change produced by the martensite transformation is accommodated through elastic deformation, this transformation is called thermoelastic martensitic transformation. An important characteristic of shape memory alloys (SMA) is the ability to undergo such a diffusionless, structural and reversible thermoelastic martensitic transformation [1]. Detailed investigations on thermoelastic martensitic transformation have been done in the fields of physics and materials science and a quite complete theoretical system, which includes the transformation crystallographic theory and thermodynamics etc., has been established by Wechsler *et al.* [2], Wayman [3], Bowles and Mackenzie [4], Delaey *et al.* [5], Christian [6], James [7], Ball and James [8], Bhattacharya [9], Abeyaratne *et al.* [10,11], and many others. With the increasing application of SMA and structural ceramics, the study on the constitutive relation of the materials with thermoelastic martensitic transformation attracts interest of the researchers of solid mechanics and a lot of work has been done by Falk [12], Patoor *et al.* [13], Abeyaratne *et al.* [10,11], Muller and Xu [14], Chu and James [15], Tanaka *et al.* [16,17], Liang *et al.* [18], Sun and Hwang [19,20], Fischer *et*

*al.* [21,22], Yan *et al.* [23–25], Song *et al.* [26], Chen *et al.* [27,28], Lu and Weng [29] and many others.

In the light of the directions of the process and the change in material microstructures, thermoelastic martensitic transformation can be divided into three kinds [5]: the forward transformation ( $p \rightarrow m$ , i.e. the transformation from parent phase to martensite), the reverse transformation ( $m \rightarrow p$ , i.e. the transformation from martensite to parent phase) and the reorientation ( $m \rightarrow m$ ) between different kinds of martensite habit plane variants. These changes in microstructures lead to various macroscopic phenomena such as pseudoelasticity, shape memory effect, etc. Therefore, in order to understand the transformation constitutive behavior more clearly, it is necessary to study it in such a finer scale as the scale of variants. In the previous work (see Sun and Hwang [19,20], Yan *et al.* [23–25], Chen *et al.* [27,28]), the constitutive models of SMA and ceramics were developed under complex thermomechanical conditions and these theories were applicable directly (see, for instance, Stam *et al.* [30], Chen *et al.* [27,28]). However, due to lack of test data for SMA single crystals subject to multi-axial loading, the constitutive model for SMA single crystals has only been compared with the available experiments under uniaxial loading.

The pseudoelastic phenomena of SMA single crystals under uniaxial loading have been investigated by many authors, such as Okamoto *et al.* [31], Horikawa *et al.* [32], Shield [33], and many others.

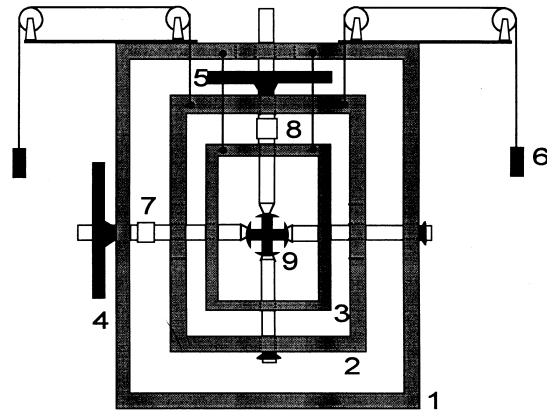
†To whom all correspondence should be addressed.

Some researchers (for instance, Sittner *et al.* [34], Tokuda *et al.* [35]) have experimentally investigated the constitutive behavior of the TiNi polycrystals under combined tension and torsion. Chu and James [15] did nice work to build biaxial setup for SMA single crystals, and observed the microstructural changes relative to the hysteresis, evolution of twins and metastability of SMA, without strain measurement. For combined tension–torsion tests of anisotropic tubular specimens cut from a single crystal rod, there arises difficulty that the strain fields are nonuniform in the circumferential direction. The biaxial test has the advantage of keeping the directions of principal stresses unchanged relative to the material. However, to the best knowledge of the authors, it seems that there have been no stress–strain tests under biaxial loading on the SMA single crystals. In this investigation, in order to verify the developed constitutive theory and to understand basic properties of thermoelastic martensitic transformation in SMA single crystals, uniaxial and biaxial loading tests under different combined loads at a constant temperature were performed on cruciform specimens of a SMA CuAlNi single crystal. The crystallographic theory for martensitic transformation developed by Wechsler *et al.* [2] has been employed to calculate the orientations of martensite variants and the transformation plastic strain. It was shown in Ref. [36] that the generalized micromechanics constitutive model proposed by Yan *et al.* [23–25] and Song *et al.* [26] can predict very well the different tensile curves as well as the kinds of martensite variants occurring in uniaxial tensile loading along different crystallographic directions of the CuAlNi SMA single crystal. In this paper experimental data of biaxial loading will be compared with theoretical predictions based on the same constitutive model. The experimental results agreed favorably with theoretical predictions.

The plan of the rest of the paper is as follows. Section 2 introduces the biaxial setup and the experimental procedure. The experimental results and discussions are demonstrated in Section 3. In Section 4, the results of the orientations and transformation plastic strain of 24 martensite variants calculated by means of the crystallographic theory for martensitic transformation are presented. For the completeness of the paper, in Section 4, the proposed micromechanics constitutive model is briefly introduced. The comparison of the theoretical predictions and experimental data is made in Section 5. The conclusions are given in Section 6.

## 2. EXPERIMENTAL PROCEDURE

The schematic structure of the biaxial loading tester designed by the authors is shown in Fig. 1. The special design of the biaxial testing device can make sure that the specimen is subjected to pure biaxial



- |                    |                   |
|--------------------|-------------------|
| 1. Main Frame      | 6. Balance        |
| 2. Middle Frame    | 7. X Force Sensor |
| 3. Inner Frame     | 8. Y Force Sensor |
| 4. X load Supplier | 9. Specimen       |
| 5. Y load Supplier |                   |

Fig. 1. Schematic structure of the biaxial tester.

loading. The possible loads are such that the principal stresses are positive and their directions remain constant. For this test the tester requires two linear jacks placed  $90^\circ$  apart. The weight of two balances equals that of the middle frame, so that the middle frame can move freely in the vertical direction. The inner frame is hung on the main frame by a soft string. The string is vertical and the inner frame can move freely in the horizontal direction. The two degrees of freedom in the horizontal and vertical directions ensure that the cruciform specimen is subjected to pure biaxial loading. If any bending or shearing is applied to the specimen, the movement of the specimen, the inner frame, and the middle frame will finally eliminate the bending or shearing effect. This special design makes it possible to get experimental results under biaxial tensile loading. Although there do exist effects of the grips on the deformation, by using the Moiré interference technique, we found that the deformation field in the central area is approximately uniform.

The composition of our specimen is Cu–13.7%, Al–4.18%, Ni–wt%. The single crystal rod was produced in the shape of a slightly-tapered cylinder with a diameter of about 23 mm and a length of about 65 mm. The cruciform specimen is obtained by cutting the cylinder transversely. The specimens were prepared in the following way. They were first heated to  $850^\circ\text{C}$  and kept at this temperature for 5 min, then drenched in the solution of 10% NaOH at room temperature ( $26.5^\circ\text{C}$ ) for 30 min. The values of transformation temperature were determined by differential scanning calorimeter (DSC) as  $M_s = -20^\circ\text{C}$ ,  $M_f = -49^\circ\text{C}$ ,  $A_s = -19^\circ\text{C}$ ,  $A_f = 0^\circ\text{C}$ . Therefore, the specimen is austenitic at room temperature. The geometry of the single crystal

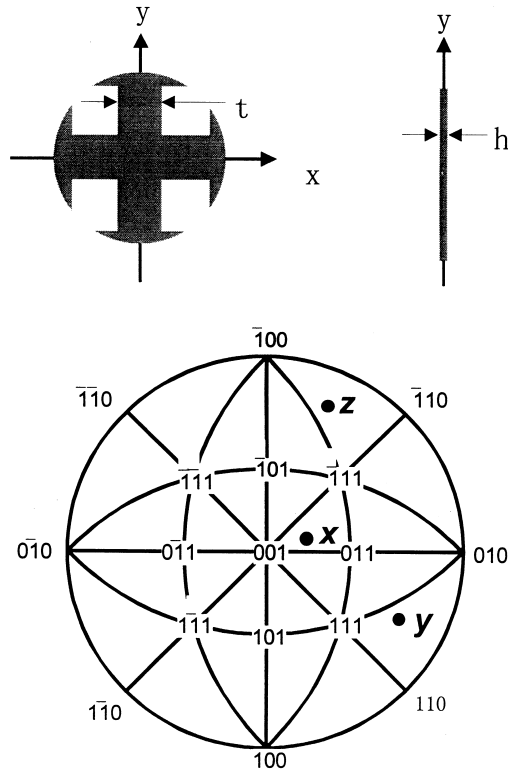


Fig. 2. (a) Geometry of the flat cruciform specimen. (b) Loading directions shown using a stereographic projection. The  $x$  direction is the horizontal loading axis, the  $y$  direction is the vertical loading axis and the  $z$  direction is the normal of the specimen.

specimen is shown in Fig. 2(a). The orientations of the specimens were detected by the X-ray back reflection Laue method. The orientations of the loading axes and the normal of the surface of the specimens relative to the parent phase can be represented by points in a stereographic projection as shown in Fig. 2(b). We specify the horizontal loading axis as the  $x$  direction, the vertical loading axis as the  $y$  direction and the normal of the surface of the specimen as the  $z$  direction. The applied loads in two directions were measured by the load cells. The stress distribution  $(\sigma_x, \sigma_y)$  in the test section of the cruciform specimen is different from the applied nominal stresses  $(s_x, s_y)$ , which are obtained through dividing the two applied loads in  $x$  and  $y$  directions by the corresponding cross-sectional area of the arm of the cruciform specimen. There have been great efforts (e.g. [37, 38]), such as presenting a series of limbs separated by slots, extending from each edge of a uniformly thinned square-shaped central region and optimizing the geometry of the cruciform specimen, aiming at homogeneity of the stress state  $(s_x, s_y)$  in the test region and at the same time  $\sigma_x \approx s_x$  and  $\sigma_y \approx s_y$ , at least for elastic case. For the specimen geometry shown in Fig. 2(a), finite element calculations show that in an isotropic elastic case (Poisson's ratio  $\nu = 0.3$ ) there is a

region of size of about 6 mm at least at the test section where the stress state  $(\sigma_x, \sigma_y)$  is rather uniform with the error of 5% and the values of the stress  $(\sigma_x, \sigma_y)$  are related to the nominal stress  $(s_x, s_y)$  by the relation:

$$\begin{aligned}\sigma_x &= 0.8908s_x - 0.1616s_y \\ \sigma_y &= -0.1616s_x + 0.8908s_y.\end{aligned}\quad (1)$$

We have tried both comparing  $s_x$ - $\varepsilon_x$  curves as shown in Fig. 3 and comparing the theoretically predicted and the measured  $\sigma_x$ - $\varepsilon_x$  curves as shown in Figs 7 and 8. We will show the experimental results in the former set of data in Section 3 and the comparison of theoretical calculation and experiment in the latter set of data in Section 5. We found that both ways of comparing lead to all the same conclusions about agreement of theoretical predictions and experiment. This is why we avoided the difficult task of analyzing the stress distribution in the test region of the cruciform specimen with accompanying martensite transformation.

The overall strains in the  $x$  and  $y$  directions were measured simultaneously by two metal foil strain gages bounded to the specimen. One is to measure the strain in the  $x$  direction and the other in the  $y$  direction. The strain gages were attached to the specimen with a special glue and by means of a special heat treatment, which can make sure that the strain gages can measure large strain accurately up to 12% in elongation. Two types of loading programs are used in our experiments. Figure 4(a) shows the loading path A:  $y$  loading  $\rightarrow x$  loading  $\rightarrow y$  unloading  $\rightarrow x$  unloading, and Fig. 4(b) illustrates the loading path B:  $x$  loading  $\rightarrow y$  loading  $\rightarrow x$  unloading  $\rightarrow y$  unloading.

### 3. EXPERIMENTAL RESULTS

The measured stress-strain curves in  $x$  direction subjected to several prescribed constant preloadings in  $y$  direction are shown in Fig. 3. A hysteresis loop of the stress-strain curve appears during loading

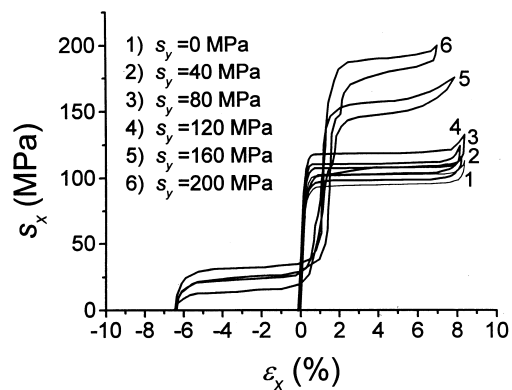


Fig. 3. Measured stress-strain curves at different values of  $\sigma_y$  under biaxial loading.

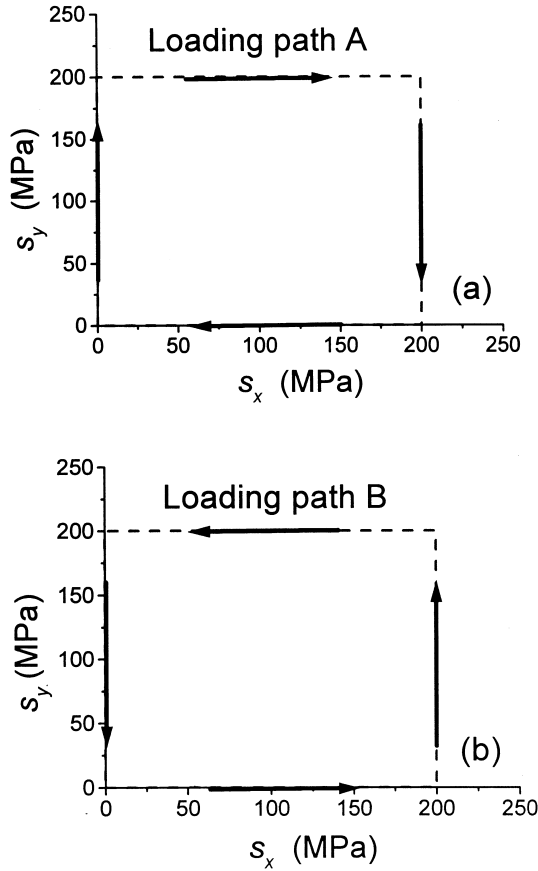


Fig. 4. (a) Stress path for loading path A with loading order:  $y$  loading  $\rightarrow$   $x$  loading  $\rightarrow$   $y$  unloading  $\rightarrow$   $x$  unloading; (b) stress path for loading path B with loading order:  $x$  loading  $\rightarrow$   $y$  loading  $\rightarrow$   $x$  unloading  $\rightarrow$   $y$  unloading.

and unloading processes. The area surrounded by the hysteresis loop represents the dissipated strain energy, and the area below the unloading curve corresponds to the recoverable strain energy. One of the main purposes of our experiments is to figure out how significantly the preload imposed in the  $y$  direction influences the stress–strain curves in the  $x$  direction. The loading process is specified as: a tensile preload is firstly applied in the  $y$  direction of the cruciform specimen until it reaches a designated value, and then it keeps constant. Furthermore, a tensile load is applied in the  $x$  direction. We recorded the stress–strain curves in the  $x$  direction at different values of  $s_y$  ( $=0, 40, 80, 120, 160, 200$  MPa). It can be found that the transformation stresses at which the transformation starts are increased as the values of load  $s_y$  are increased. When  $s_y$  is zero, the loading is uniaxial. When  $s_y$  is not too high, the shape of the stress–strain curves has no substantial change relative to the stress–strain curve of uniaxial loading, except that there is an elastic contraction before loading in the  $x$  direction. The curves are mainly linear below the transformation stress. The curve shows a clear plateau at the transformation stress. This is due to the trans-

formation from austenite to martensite. When the stress induced martensitic transformation finishes, the slope of the curve begins to increase again. However, when  $s_y$  is high enough, the shape of the curve changes significantly, as shown in Fig. 3. It is found that  $\epsilon_x$  has very high initial values about  $-6\%$  before the stress in the  $x$  direction is applied. This is because the high preload in the  $y$  direction has caused phase transition before the load in the  $x$  direction is applied. Then, if we apply a load in the  $x$  direction, a small load can lead to a plateau due to reorientation of martensite variants. A second flat plateau appears when  $s_x$  reaches another critical value. It is important to point out that the transformation mechanism in the case of applying a low  $s_y$  is quite different from that in the case of applying a high  $s_y$ . In the case of a low  $s_y$ , only one flat plateau is caused by the forward and reverse martensite transformations, while both of two flat plateaus in the case of a high  $s_y$  are caused by the reorientation among martensite variants. From Fig. 3 we can also find that the deformation is anisotropic because the transformation stress in the  $y$  direction is much higher than that in the  $x$  direction under uniaxial loading. For example, when  $s_y=0$ , the value of stress  $s_x$  at start of transformation under uniaxial tension in the  $x$ -direction equals 102 MPa. When  $s_y=120$  MPa, there is no martensitic transformation in the  $y$  direction, but the transformation appears when  $s_y=160$  MPa. This means that the value of uniaxial tension loading  $s_y$  at start of transformation is larger than 120 MPa but less than 160 MPa and is not equal to the value of uniaxial tension loading  $s_x$  at start of transformation.

#### 4. MICROSCOPIC TRANSFORMATION INDUCED STRAIN

In the proposed micromechanics constitutive model, the microscopic transformation plastic strain has to be calculated at first. By use of the crystallographic theory for martensitic transformation developed by Wechsler *et al.* [2] and Bowles and Mackenzie [4], and in terms of the measured lattice values of CuAlNi, the habit planes of the 24 variants and the transformation induced strains for the 24 variants can be predicted by calculation. According to the crystallographic theory, the martensitic transformation is realized through an invariant plane strain, which is a terminology of materials science and is actually a kind of deformation gradient tensor in the light of continuum mechanics. As shown in Fig. 5, the invariant plane strain (i.e. deformation gradient tensor)  $\mathbf{D}$  can be expressed by

$$\mathbf{D} = \mathbf{I} + \text{gen} \quad (2)$$

where  $\mathbf{I}$  is the identity tensor of rank two,  $\mathbf{e}$  is the unit vector along displacement direction of the invariant plane,  $\mathbf{n}$  is the unit vector normal to the

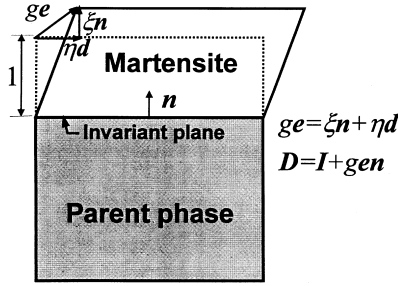


Fig. 5. Illustration of an invariant plane strain.

invariant plane, and  $g$  is the displacement magnitude of the invariant plane per unit length along the normal  $\mathbf{n}$ . According to the small deformation theory, the corresponding transformation strain  $\varepsilon^p$  can be easily written as

$$\varepsilon^p = \frac{1}{2}g(\mathbf{en} + \mathbf{ne}). \quad (3)$$

We define

$$\mathbf{R} = \frac{1}{2}(\mathbf{en} + \mathbf{ne}) \quad (4)$$

where  $\mathbf{R}$  is called the orientation tensor of the martensite variant. In terms of the crystallographic theory for martensitic transformation, we can determine all the possible kinds of martensite variants with different orientations. The orientation tensor  $\mathbf{R}_s$  of the  $s$ th kind of variants (crystallographically permissible) can be obtained by equation (4). Thus, we can calculate the microscopic transformation strain corresponding to the  $s$ th kind of variants by

$$\varepsilon_s^p = g\mathbf{R}_s = \frac{1}{2}g(\mathbf{e}_s\mathbf{n}_s + \mathbf{n}_s\mathbf{e}_s) \quad (s = 1, \dots, N) \quad (5)$$

where  $N$  is the number of kinds of variants. Table 1 gives the normals of the habit planes of the 24 kinds of variants expressed in the crystallographic directions of the parent phase. Table 2 gives the transformation strains of the 24 kinds of variants expressed in the crystallographic directions of the parent phase as well.

##### 5. A CONSTITUTIVE MODEL FOR SINGLE CRYSTAL SMA

In the next section our experimental results will be compared with the constitutive models proposed by Yan *et al.* [23–25], and Song *et al.* [26]. It must be pointed out that due to the possibility of transformation softening, the general constitutive relation was given only in strain space in the formulation of Yan *et al.* Therefore, in this section we shall formulate the stress–strain relation in stress space in order to compare the theoretical prediction with the experiments. Referring the details to the original papers, the basic assumptions and the main formulation of the theory are presented below.

In order to establish the transformation constitutive model, a representative material sample (constitutive element) with volume  $V$  shown in Fig. 6 is taken from a single crystalline bulk. A temperature  $T$  is uniformly distributed everywhere in the element and the external macroscopic stress  $\Sigma$  or strain  $\mathbf{E}$  is applied on the boundary. With the change of temperature  $T$  or stress  $\Sigma$  or strain  $\mathbf{E}$ , the transformation and/or variant reorientation may happen. Some kinds of martensitic variants with different orientations will emerge in the element during transformation and some differently oriented martensitic variants will coalesce when reorientation happens. Due to the incompatibility of the transformation strain of the variants with the surrounding elastic parent matrix, internal stress will be aroused and elastic strain energy will be stored in a constitutive element. Many investigators (e.g. [3, 39]) showed that such kind of elastic strain energy plays a very important role in the thermodynamics and kinetics of thermoelastic martensitic transformation. For example, the stored elastic energy usually opposes the forward transformation and assists the reverse transformation (as the driving force). In the proposed model, in order to analyze the elastic strain energy in the constitutive element, a concept of inclusion was used. Inclusions are defined as the very small transformed martensite variants. A lot of micrographs show that a martensite variant appears in a shape of plate or blade, so the geometric shape of a variant inclusion may be approximated as an oblate spheroid. We further assume that the short axis of the spherical inclusion is normal to the invariant plane of the variant. So different kinds of variants are represented by inclusions with different orientations of the short axes. A constitutive element is composed of the parent phase and a large number of inclusions, and the inclusions are considered to be located stochastically as the external

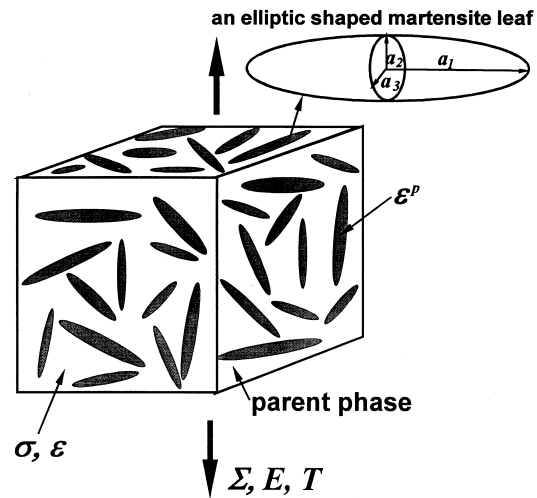


Fig. 6. Illustration of a constitutive element with elliptic shaped martensite leaves.

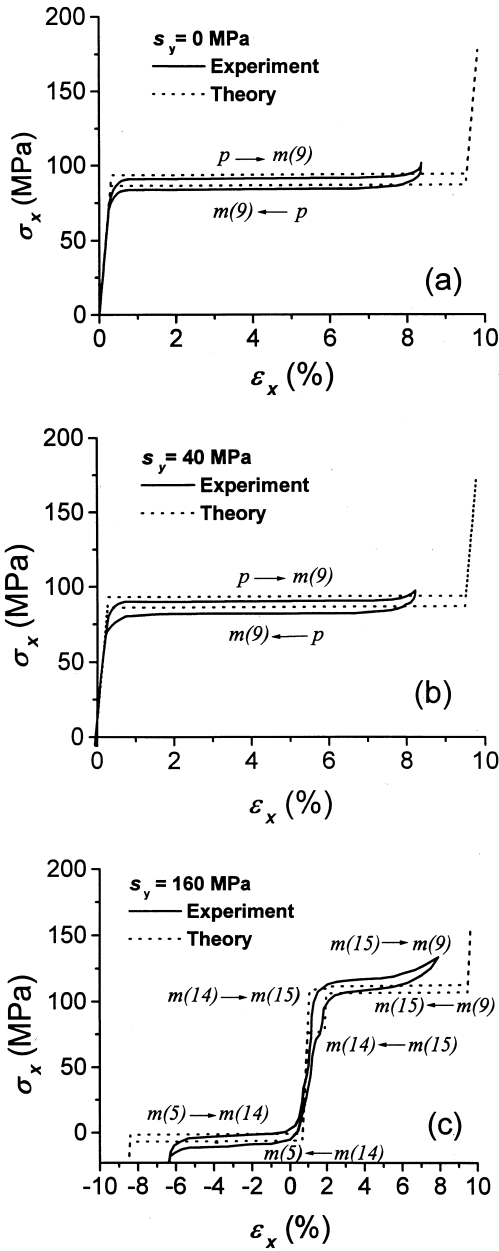


Fig. 7. Comparison of the calculated stress–strain curve and measured stress–strain curve. (a)  $\sigma_y=0$ , (b)  $\sigma_y=40$  MPa, (c)  $\sigma_y=160$  MPa. The calculations were made by the model without considering the surface energy change.

stress or strain is homogeneous. Therefore, the forward transformation is just the process in which the number of inclusions or the total volume fraction of all various  $N$  kinds of inclusions increase continuously, while the reverse transformation is the process with the number of inclusions decreasing and the reorientation is the process with the change of volume fractions between different kinds of variants.

Denote the volume occupied by the  $s$ th kind of variants ( $s = 1, \dots, N$ ) by  $V_s$ , and the corresponding volume fraction by  $f_s (= V_s/V)$ . The total volume of

transformed variants  $V_i$ , total volume fraction  $f$  and the volume of the parent phase  $V_p$  are:

$$V_i = \sum_{s=1}^N V_s \quad f = \sum_{s=1}^N f_s \quad V_p = V - V_i. \quad (6)$$

Under the applied global macroscopic stress  $\Sigma$  and temperature  $T$ , the microscopic stress and strain in the element are expressed by  $\sigma$  and  $\epsilon$ . Then there exists the relation between  $\sigma$  and  $\Sigma$ ,

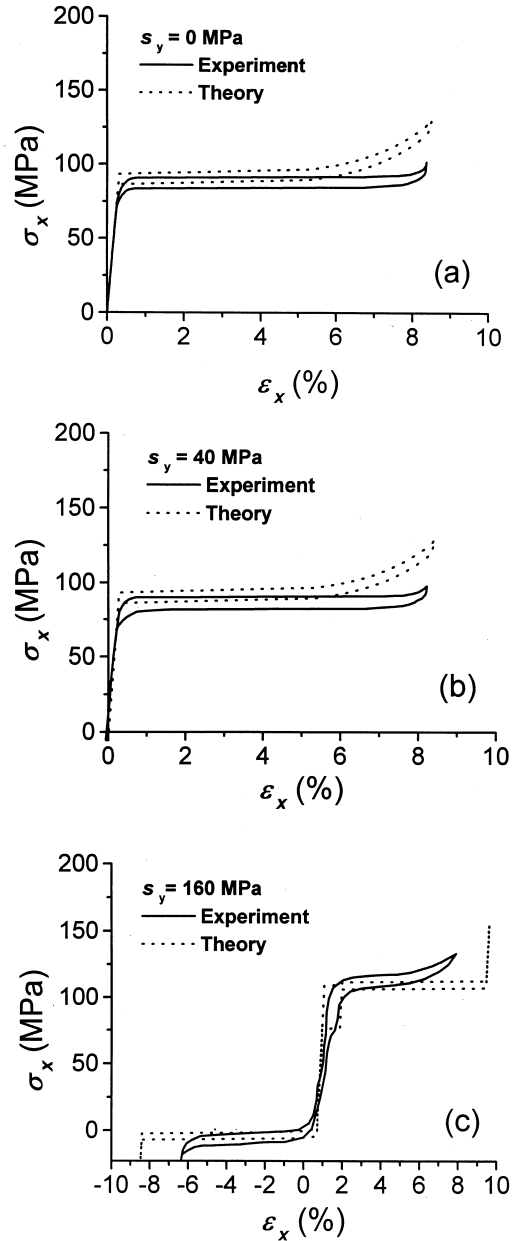


Fig. 8. Comparison of the calculated stress–strain curve and measured stress–strain curve (a)  $\sigma_y=0$ , (b)  $\sigma_y=40$  MPa, (c)  $\sigma_y=160$  MPa. The calculations were made by the model considering the surface energy change.

Table 1. Normal directions of the habit planes of the 24 variants

Variant no.	$n_1$	$n_2$	$n_3$
1	4.98019940224e-02	6.83513821586e-01	7.28236649100e-01
2	4.98019940224e-02	-6.83513821586e-01	7.28236649100e-01
3	-4.98019940224e-02	6.83513821586e-01	7.28236649100e-01
4	-4.98019940224e-02	-6.83513821586e-01	7.28236649100e-01
5	4.98019940224e-02	7.28236649100e-01	6.83513821586e-01
6	4.98019940224e-02	-7.28236649100e-01	6.83513821586e-01
7	-4.98019940224e-02	7.28236649100e-01	6.83513821586e-01
8	-4.98019940224e-02	-7.28236649100e-01	6.83513821586e-01
9	6.83513821586e-01	4.98019940224e-02	7.28236649100e-01
10	6.83513821586e-01	-4.98019940224e-02	7.28236649100e-01
11	-6.83513821586e-01	4.98019940224e-02	7.28236649100e-01
12	-6.83513821586e-01	-4.98019940224e-02	7.28236649100e-01
13	6.83513821586e-01	7.28236649100e-01	4.98019940224e-02
14	6.83513821586e-01	-7.28236649100e-01	4.98019940224e-02
15	-6.83513821586e-01	7.28236649100e-01	4.98019940224e-02
16	-6.83513821586e-01	-7.28236649100e-01	4.98019940224e-02
17	7.28236649100e-01	4.98019940224e-02	6.83513821586e-01
18	7.28236649100e-01	-4.98019940224e-02	6.83513821586e-01
19	-7.28236649100e-01	4.98019940224e-02	6.83513821586e-01
20	-7.28236649100e-01	-4.98019940224e-02	6.83513821586e-01
21	7.28236649100e-01	6.83513821586e-01	4.98019940224e-02
22	7.28236649100e-01	-6.83513821586e-01	4.98019940224e-02
23	-7.28236649100e-01	6.83513821586e-01	4.98019940224e-02
24	-7.28236649100e-01	-6.83513821586e-01	4.98019940224e-02

$$\begin{aligned} \boldsymbol{\Sigma} &= \langle \boldsymbol{\sigma} \rangle_V = \frac{1}{V} \int_V \boldsymbol{\sigma} \, dV \\ &= \sum_{s=1}^N f_s \langle \boldsymbol{\sigma} \rangle_{V_s} + (1-f) \langle \boldsymbol{\sigma} \rangle_{V_p} \end{aligned} \quad (7)$$

where  $\langle \cdot \rangle$  denotes volume average over the volume indicated by the subscript. The microscopic and macroscopic strains are assumed to be small and can therefore be decomposed into elastic and plastic parts:

$$\mathbf{E} = \langle \boldsymbol{\epsilon}^e \rangle_V + \langle \boldsymbol{\epsilon}^p \rangle_V = \mathbf{E}^e + \mathbf{E}^p = \mathbf{M} : \boldsymbol{\Sigma} + \mathbf{E}^p \quad (8)$$

where  $\mathbf{M}$  is the elastic compliance tensor. According to the crystallographic theory of martensitic trans-

formation, we have

$$\mathbf{E}^p = \sum_{s=1}^N f_s \boldsymbol{\epsilon}_s^p = g \sum_{s=1}^N f_s \mathbf{R}_s. \quad (9)$$

By using Mori–Tanaka mean field theory [40], the elastic strain energy induced by internal stress in a unit volume of the element can be calculated [41] as

$$\begin{aligned} W^* &= -\frac{1}{2} \sum_{s=1}^N f_s \boldsymbol{\epsilon}_s^p : \mathbf{L} : (\mathbf{S}_s - \mathbf{I}) : \boldsymbol{\epsilon}_s^p \\ &+ \frac{1}{2} \sum_{s=1}^N \sum_{t=1}^N f_s f_t \boldsymbol{\epsilon}_s^p : \mathbf{L} : (\mathbf{S}_t - \mathbf{I}) : \boldsymbol{\epsilon}_s^p \end{aligned} \quad (10)$$

Table 2. Transformation strains of the 24 variants

Variant no.	$\epsilon_{11}^p$	$\epsilon_{12}^p$	$\epsilon_{22}^p$	$\epsilon_{13}^p$	$\epsilon_{23}^p$	$\epsilon_{33}^p$
1	4.61625e-04	-6.86274e-04	-1.05792e-01	6.84996e-03	-8.66572e-03	1.01624e-01
2	4.61625e-04	6.86274e-04	-1.05792e-01	6.84996e-03	8.66572e-03	1.01624e-01
3	4.61625e-04	6.86274e-04	-1.05792e-01	-6.84996e-03	-8.66572e-03	1.01624e-01
4	4.61625e-04	-6.86274e-04	-1.05792e-01	-6.84996e-03	8.66572e-03	1.01624e-01
5	4.61625e-04	6.84996e-03	1.01624e-01	-6.86274e-04	-8.66572e-03	-1.05792e-01
6	4.61625e-04	-6.84996e-03	1.01624e-01	-6.86274e-04	8.66572e-03	-1.05792e-01
7	4.61625e-04	-6.84996e-03	1.01624e-01	6.86274e-04	-8.66572e-03	-1.05792e-01
8	4.61625e-04	6.84996e-03	1.01624e-01	6.86274e-04	8.66572e-03	-1.05792e-01
9	-1.05792e-01	-6.86274e-04	4.61625e-04	-8.66572e-03	6.84996e-03	1.01624e-01
10	-1.05792e-01	6.86274e-04	4.61625e-04	-8.66572e-03	-6.84996e-03	1.01624e-01
11	-1.05792e-01	6.86274e-04	4.61625e-04	8.66572e-03	6.84996e-03	1.01624e-01
12	-1.05792e-01	-6.86274e-04	4.61625e-04	8.66572e-03	-6.84996e-03	1.01624e-01
13	-1.05792e-01	-8.66572e-03	1.01624e-01	-6.86274e-04	6.84996e-03	4.61625e-04
14	-1.05792e-01	8.66572e-03	1.01624e-01	-6.86274e-04	-6.84996e-03	4.61625e-04
15	-1.05792e-01	8.66572e-03	1.01624e-01	6.86274e-04	6.84996e-03	4.61625e-04
16	-1.05792e-01	-8.66572e-03	1.01624e-01	6.86274e-04	-6.84996e-03	4.61625e-04
17	1.01624e-01	6.84996e-03	4.61625e-04	-8.66572e-03	-6.86274e-04	-1.05792e-01
18	1.01624e-01	-6.84996e-03	4.61625e-04	-8.66572e-03	6.86274e-04	-1.05792e-01
19	1.01624e-01	-6.84996e-03	4.61625e-04	8.66572e-03	-6.86274e-04	-1.05792e-01
20	1.01624e-01	6.84996e-03	4.61625e-04	8.66572e-03	6.86274e-04	-1.05792e-01
21	1.01624e-01	-8.66572e-03	-1.05792e-01	6.84996e-03	-6.86274e-04	4.61625e-04
22	1.01624e-01	8.66572e-03	-1.05792e-01	6.84996e-03	6.86274e-04	4.61625e-04
23	1.01624e-01	8.66572e-03	-1.05792e-01	-6.84996e-03	-6.86274e-04	4.61625e-04
24	1.01624e-01	-8.66572e-03	-1.05792e-01	-6.84996e-03	6.86274e-04	4.61625e-04

where  $\mathbf{I}$  is the identity tensor,  $\mathbf{L}$  is the constant elastic stiffness tensor of the element and  $\mathbf{S}_t$  is the Eshelby tensor for  $t$ th kind of variant ( $t = 1, 2, \dots, N$ ), determined by elastic constants and the shape parameters. Defining

$$W_s = -\frac{1}{2} \boldsymbol{\varepsilon}_s^p : \mathbf{L} : (\mathbf{S}_s - \mathbf{I}) : \boldsymbol{\varepsilon}_s^p \quad (11)$$

$$W_{st} = -\frac{1}{2} \boldsymbol{\varepsilon}_s^p : \mathbf{L} : (\mathbf{S}_t - \mathbf{I}) : \boldsymbol{\varepsilon}_t^p \quad (12)$$

we have

$$W^* = \sum_{s=1}^N f_s W_s - \sum_{s=1}^N \sum_{t=1}^N f_s f_t W_{st}. \quad (13)$$

For any two kinds of variants  $s$  and  $t$ , usually  $W_{st} \neq W_{ts}$  ( $s, t = 1, 2, \dots, N$ ). For convenience in mathematical treatment, we define a symmetric matrix as

$$\tilde{W}_{st} = \frac{1}{2} (W_{st} + W_{ts}). \quad (14)$$

When  $s = t$ , we have

$$W_{ss} = W_s = W_t \quad (s, t = 1, \dots, N). \quad (15)$$

Assume the elastic stiffness tensor  $\mathbf{L}$  is isotropic, then  $W_s$  ( $s = 1, 2, \dots, N$ ) are all equal and can be denoted by  $W_i$  (subscript  $i$  for ‘‘inclusion’’). Equation (13) can be rewritten as

$$W^* = W_i \sum_{s=1}^N f_s - \sum_{s=1}^N \sum_{t=1}^N f_s f_t \tilde{W}_{st}. \quad (16)$$

The total elastic strain energy  $W$  per unit volume of the constitutive element can be expressed by

$$\begin{aligned} W &= \frac{1}{2} \boldsymbol{\Sigma} : \mathbf{M} : \boldsymbol{\Sigma} + W^* \\ &= \frac{1}{2} \left( \mathbf{E} - \sum_{s=1}^N \boldsymbol{\varepsilon}_s^p f_s \right) : \mathbf{L} : \left( \mathbf{E} - \sum_{s=1}^N \boldsymbol{\varepsilon}_s^p f_s \right) \\ &\quad + W_i \sum_{s=1}^N f_s - \sum_{s=1}^N \sum_{t=1}^N f_s f_t \tilde{W}_{st}. \end{aligned} \quad (17)$$

As all the  $p$ - $m$  and  $m$ - $m$  interfaces are coherent during martensitic transformation, the surface energy change is ignored. The total change in chemical free energy  $\Delta G_{\text{chem}}$  for unit volume of the constitutive element is

$$\begin{aligned} \Delta G_{\text{chem}} &= \frac{\Delta G}{V} \sum_{s=1}^N V_s \\ &= \Delta G \sum_{s=1}^N f_s \approx K(T - T_0) \sum_{s=1}^N f_s \end{aligned} \quad (18)$$

where  $T_0$  is the equilibrium temperature of the two phases and  $k$  is a positive material constant. The Helmholtz free energy  $\Phi$  and the complementary free energy  $\Psi$  of the constitutive element per unit volume can be formulated, respectively, as

$$\begin{aligned} \Phi(\mathbf{E}, T, f_1, \dots, f_N) &= W + \Delta G_{\text{chem}} \\ &= \frac{1}{2} \left( \mathbf{E} - \sum_{s=1}^N \boldsymbol{\varepsilon}_s^p f_s \right) : \mathbf{L} : \left( \mathbf{E} - \sum_{s=1}^N \boldsymbol{\varepsilon}_s^p f_s \right) \\ &\quad + (W_i + \Delta G) \sum_{s=1}^N f_s - \sum_{s=1}^N \sum_{t=1}^N f_s f_t \tilde{W}_{st} \end{aligned} \quad (19)$$

$$\begin{aligned} \Psi(\boldsymbol{\Sigma}, T, f_1, \dots, f_N) &= -(W + \Delta G_{\text{chem}} - \boldsymbol{\Sigma} : \mathbf{E}) \\ &= \frac{1}{2} \boldsymbol{\Sigma} : \mathbf{M} : \boldsymbol{\Sigma} + \boldsymbol{\Sigma} : \sum_{s=1}^N \boldsymbol{\varepsilon}_s^p f_s \\ &\quad - (W_i + \Delta G) \sum_{s=1}^N f_s + \sum_{s=1}^N \sum_{t=1}^N f_s f_t \tilde{W}_{st}. \end{aligned} \quad (20)$$

In order to determine the transformation yield condition and the reorientation yield condition, it is necessary to analyze the energy dissipation during transformation and reorientation. The total energy dissipation  $W_d$  of unit volume of the constitutive element is the summation of the energy dissipation  $W_d^{\text{tr}}$  per unit volume of the constitutive element during the forward and/or reverse transformation and the energy dissipation  $W_d^{\text{re}}$  per unit volume of the constitutive element during the reorientation. We assumed that  $W_d^{\text{tr}}$  is proportional to the accumulated volume fraction of transformation and  $W_d^{\text{re}}$  proportional to the accumulated volume fraction of reorientation. Then, we have:

$$\begin{aligned} W_d &= W_d^{\text{tr}} + W_d^{\text{re}} = D^{\text{tr}} f_{cu}^{\text{tr}} + D^{\text{ve}} f_{cu}^{\text{re}} \\ &= D^{\text{tr}} \sum_{s=1}^N \int_0^{f_{s0}} |df_{s0}| + \frac{1}{2} D^{\text{re}} \sum_{s=1}^N \sum_{\substack{t=1 \\ t \neq s}}^N \int_0^{f_{st}} |df_{st}| \end{aligned} \quad (21)$$

where  $D^{\text{tr}}$ ,  $D^{\text{re}}$  can be considered, respectively, as generalized frictional resistance to the  $p$ - $m$  and the  $m$ - $m$  interface motion, and they are assumed to be material constants.  $\dot{f}_{s0} = df_{s0}/dt$  is the rate of change of the volume fraction of the  $s$ th kind of variants from the parent phase ( $f_{s0} > 0$  for forward and  $f_{s0}$  for reverse transformation), and  $\dot{f}_{st}$  ( $s \neq t$ ) is the rate of change of the volume fraction of the  $s$ th kind of variants reoriented from the  $t$ th kind of variants ( $\dot{f}_{st} = -\dot{f}_{ts}$ ). Denoting the thermodynamic force conjugate to the internal variable  $f_s$  by  $F_s$ , then  $F_s = \partial \Psi / \partial f_s$ . According to the thermodynamics,

$$\dot{\Psi}|_{\boldsymbol{\Sigma}, T} = \sum_{s=1}^N \frac{\partial \Psi}{\partial f_s} \dot{f}_s = \dot{W}_d. \quad (22)$$

Substituting equation (20) for  $\Psi$  and equation (21) for  $W_d$  in equation (22), and equating the coefficients of nonvanishing rates of change of volume fractions, we can get the following forward and reverse transformations yield conditions  $Y_{s0}$  for the  $s$ th kind of martensite variants and the reorientation conditions  $Y_{st}$  for the  $t$ th kind of variants to be reoriented to the  $s$ th variants. They are expressed by

$$Y_{s0}(\Sigma, T, f_1, \dots, f_N) = \mathbf{\epsilon}_s^p : \Sigma + 2 \sum_{n=1}^N \tilde{W}_{sn} f_n - (W_i + \Delta G) \mp D^{\text{tr}} = 0 \quad (s = 1, \dots, N) \quad (23)$$

$$Y_{st}(\Sigma, T, f_1, \dots, f_N) = (\mathbf{\epsilon}_s^p - \mathbf{\epsilon}_t^p) : \Sigma + 2 \sum_{n=1}^N (\tilde{W}_{sn} - \tilde{W}_{tn}) f_n - D^{\text{re}} = 0 \quad (s = 1, \dots, N; \quad t = 1, \dots, s-1, s+1, \dots, N). \quad (24)$$

In equation (23) the upper (lower) sign corresponds to the forward (reverse) transformation. According to the internal variable theory [42], the constitutive relation can be expressed by

$$\dot{\mathbf{E}} = \mathbf{M} : \dot{\Sigma} + \sum_{s=1}^N \frac{\partial F_s}{\partial \Sigma} \dot{f}_s = \mathbf{M} : \dot{\Sigma} + \sum_{s=1}^N \mathbf{\epsilon}_s^p \dot{f}_s \quad (s = 1, \dots, N) \quad (25)$$

where

$$\dot{f}_s = \dot{f}_{s0} + \dot{f}_{s1} + \dots + \dot{f}_{s(s-1)} + \dot{f}_{s(s+1)} + \dots + \dot{f}_{sN} \quad (s = 1, \dots, N). \quad (26)$$

In order for the processes of forward transformation, reverse transformation and reorientation to happen simultaneously, the macroscopic stress rate  $\dot{\Sigma}$ , the temperature rate  $\dot{T}$  and the volume fraction rates  $\dot{f}_n$  must satisfy the following consistency equations:

$$\begin{aligned} \dot{Y}_{s0} &= 0 \\ \dot{Y}_{st} &= 0 \end{aligned} \quad (27)$$

or

$$\mathbf{\epsilon}_s^p : \dot{\Sigma} - k \dot{T} = -2 \sum_{n=1}^N \left( \tilde{W}_{sn} \dot{f}_{n0} + \sum_{q \in \{B_n\}} (\tilde{W}_{sn} - \tilde{W}_{sq}) \dot{f}_{nq} \right) \quad (s \in \{A\}) \quad (28)$$

$$\begin{aligned} (\mathbf{\epsilon}_s^p - \mathbf{\epsilon}_t^p) : \dot{\Sigma} &= -2 \sum_{n=1}^N (\tilde{W}_{sn} - \tilde{W}_{tn}) \dot{f}_{n0} \\ &- \sum_{n=1}^N \sum_{q \in \{B_n\}} (\tilde{W}_{sn} - \tilde{W}_{tn} - \tilde{W}_{sq} + \tilde{W}_{tq}) \dot{f}_{nq} \\ &(s = 1, \dots, N; \quad t \in \{B_s\}) \end{aligned} \quad (29)$$

where  $\{A\}$  is the set  $\{s; \dot{f}_{s0} \neq 0\}$  of the active kinds of variants with forward or reverse transformation happening and  $\{B_s\}$  is the set of  $\{t; t \neq s \text{ and } \dot{f}_{st} \neq 0\}$  of the active kinds of variants which are reoriented to or from the  $s$ th kind of variants. After calculating  $\dot{f}_s$  ( $s = 1, \dots, N$ ) from equation (26), we can obtain the macroscopic strain rate  $\dot{\mathbf{E}}$  by using equation (25).

## 6. COMPARISON OF THE THEORY AND EXPERIMENTS

Now we turn to the calculation of the overall stress-strain curve by use of the above theory. Yan *et al.* [23–25] assumed that  $D^{\text{tr}}$ ,  $D^{\text{re}}$  are material constants and can be calculated from the area of the domain encircled by the pseudoelastic hysteresis curves. They have proved that  $D^{\text{tr}}$  equals the half of the area of the domain encircled by the pseudoelastic hysteresis loop measured during the forward and reverse transformation, as shown by solid lines in Fig. 7(a) or 7(b), and  $D^{\text{re}}$  is equal to the half of the area of the domain encircled by the pseudoelastic hysteresis loop measured during reorientation, as shown in Fig. 7(c). All the material parameters are deduced from relevant test results:  $D^{\text{tr}} = 0.28$  MPa,  $D^{\text{re}} = 0.16$  MPa,  $k = 0.23$  MPa/°C [32],  $M_s = -20^\circ\text{C}$ ,  $M_f = -49^\circ\text{C}$ ,  $A_s = -19^\circ\text{C}$ ,  $A_f = 0^\circ\text{C}$ ,  $T_0 = (M_s + A_s)/2 = -19.5^\circ\text{C}$ . The shape of transformed inclusions is assumed to be flat ellipsoid. The transformation strains for 24 martensitic variants are listed in Table 2. The elastic compliance constants are  $M_{1111} = 4.49 \times 10^{-5}$ /MPa,  $M_{1122} = -2.12 \times 10^{-5}$ /MPa,  $M_{1212} = 0.51 \times 10^{-5}$ /MPa. Relative to the crystallographic directions of the parent phase, the loading directions are  $(-0.0925, 0.3698, 0.9245)$  along the  $x$  axis and  $(0.4268, 0.8536, -0.2988)$  along the  $y$  axis, respectively.

Figure 7 shows the comparison between the theoretical results (dotted line) and the experimental data (solid line). Figure 7(a) is the case for  $s_y = 0$ , and theoretical result shows that variant no. 9 appears during loading in the  $x$  axis ( $p \rightarrow m(9)$ ) and variant no. 9 disappears during unloading in the  $x$  axis ( $m(9) \rightarrow p$ ). Variant no. 9 has such a normal of the habit plane listed in Table 1 as  $(0.68351382, 0.04980199, 0.72823665)$  with regard to the crystallographic direction of the parent phase ( $p$ ), and its transformation strains are listed in the ninth line of Table 2. In Fig. 7(b),  $s_y = 40$  MPa, we can find that the value of  $s_y$  is not large enough to produce the transformation, so that there is still an elastic stage

during loading in  $x$ -direction. The theoretical calculation also predicts that no variant appears during loading in the  $y$  axis, but variant no. 9 appears during loading in the  $x$  axis ( $p \rightarrow m(9)$ ) and disappears during unloading in the  $x$  axis ( $m(9) \rightarrow p$ ). The calculation indicates that when  $s_y$  is small, the pseudoelasticity of the single crystal is due mainly to the transformation between austenite and martensite. In this case, only one variant appears during the loading and unloading processes. In Fig. 7(c),  $s_y = 160$  MPa, it is obvious that the value of  $s_y$  is large enough to produce the transformation, so that in the  $\sigma_y \sim \varepsilon_y$  diagram (not shown here in the figure) there appears a plateau of the pseudoelastic hysteresis loop before loading in the  $x$  direction. The theoretical prediction indicates that variant no. 5 appears during loading in the  $y$  axis ( $p \rightarrow m(5)$ ). During loading and unloading in the  $x$  axis, the following transformation sequence occurs:  $m(5) \rightarrow m(14)$ ,  $m(14) \rightarrow m(15)$ ,  $m(15) \rightarrow m(9)$ ,  $m(9) \rightarrow m(15)$ ,  $m(15) \rightarrow m(14)$ ,  $m(14) \rightarrow m(5)$ . The normal of the habit planes and the transformation strains for variant no. 5, 9, 14 and 15 are listed in Table 1, respectively. Variant no. 5 finally disappears during unloading in the  $y$  axis ( $m(5) \rightarrow p$ ). This means that when  $\sigma_y$  is as large as to induce transformation, the pseudoelasticity in the  $x$  direction is mostly related to the reorientation among martensite variants. That is, the theory predicts the appearance of more than two variants in the history of loading and unloading, and this agrees with the experimentally observed two flat plateaux in the stress-strain curve. From the comparison shown in Fig. 7, it may be concluded that the theory is acceptable because theoretical results are close to experimental data.

As mentioned before, Yan *et al.* ignored the surface energy change in their model since they assumed that all the  $p$ - $m$  and  $m$ - $m$  interfaces are coherent for martensitic transformation. However, we find from Fig. 7 that the calculated hysteresis loop curves are almost horizontal at the values of transformation stress, which does not agree with the experiments showing significant hardening when the strain is larger than 8%. We try to examine the effect of the surface energy change. Following Song *et al.* [26], denote  $W^f$  as the surface energy between the interface of the parent phase and martensite variants:

$$W^f = (h_0 + hf^m) \quad (30)$$

where  $f$  is the volume fraction of inclusions,  $h_0$ ,  $h$  are material constants, and  $h = k(M_s - M_f)$ . Then, the complementary free energy  $\Psi$  of the constitutive element per unit volume given in equation (20) is rewritten as

$$\Psi(\Sigma, T, f_1, \dots, f_N) = - (W + \Delta G_{\text{chem}} + W^f - \Sigma : \mathbf{E}). \quad (31)$$

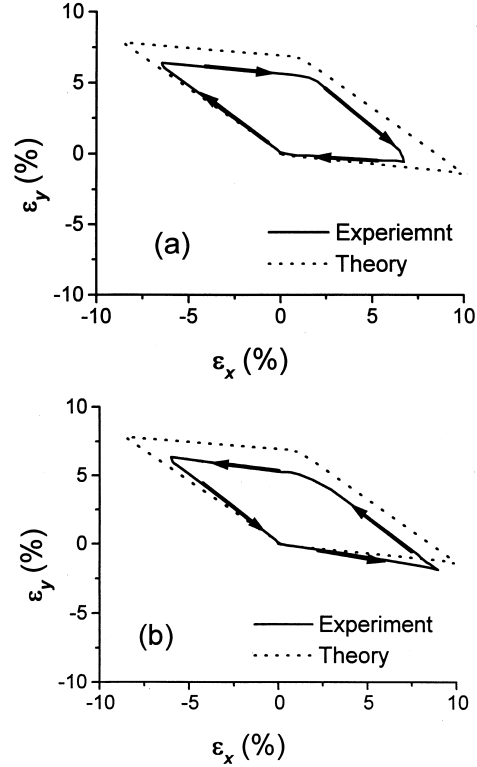


Fig. 9. Comparison of the calculated strain path and measured strain path: (a) corresponding to the loading path A as shown in Fig. 4(a); (b) corresponding to the loading path B as shown in Fig. 4(b).

Following the above procedure, we can also predict the overall stress-strain relation. In the calculation, we can use  $h_0 = 0$ ,  $m = 5$  as Song *et al.* [26] did, and other material constants are the same as before, for instance,  $k = 0.23$  MPa/ $^{\circ}\text{C}$ , and  $M_s = -20^{\circ}\text{C}$  and  $M_f = -49^{\circ}\text{C}$ , we get  $h = 6.67$  MPa. Figure 8 shows the comparison of the calculated results and the measured data. We find that when we consider the surface energy change in our model, the forward and reverse transformation will be affected, while the surface energy change does not affect the reorientation process. This is reasonable because, as well-known, the  $m$ - $m$  interfaces are coherent while the  $p$ - $m$  interfaces actually are not coherent for martensitic transformation.

We have investigated the strain paths under two types of loading paths as shown in Fig. 4. Figure 9(a) and (b) demonstrate the comparison of the calculated and measured strain paths corresponding to the loading path A and the loading path B, shown in Fig. 4(a) and (b), respectively. It can be found that the shapes of strain-paths of Fig. 9(a) and (b) seem similar, but the slopes of corresponding segments of loops are different. This is because the kinds of martensite variants occurring in loading paths A and B are different. We can conclude that the formation and reorientation of the martensite

variants are dependant upon the loading path so that the strain path relies on the loading path too.

## 7. CONCLUSIONS

The biaxial loading tests for SMA single crystals are very useful for revealing the basic characteristics of thermoelastic martensite transformation induced by stress and for verifying the constitutive models. By applying different combined loading histories on cruciform specimens, some new phenomena were observed. When the nominal loading stress  $s_y$  is not too high, the transformation stresses in the  $x$ -axis direction increase as the values of stress  $s_y$  increase, and the shape of the stress–strain curves has no substantial change relative to the stress–strain curve of uniaxial loading, except that there is an elastic contraction before loading in the  $x$  direction. When  $s_y$  is small, only the forward and reverse transformation will occur. However, when  $s_y$  is high enough to induce the transformation, the shape of the stress–strain curve for the  $x$ -axis direction changes significantly. Once  $s_y$  is over the value corresponding to the start of transformation, the reorientation takes place in the process of  $s_x$  loading. The results also indicate that the pseudoelasticity is so anisotropic that the transformation stress in the  $y$  direction is larger than that in the  $x$  direction. In addition, by use of the crystallographic theory for martensitic transformation, the habit planes of the 24 variants and the transformation plastic strain for the 24 variants of the CuAlNi single crystal are predicted. Experimental data are compared with theoretical calculation based on the generalized micromechanics constitutive model. It can be found that the model [23–26] can predict the evolutions of variants both in the forward/reverse transformation and in the reorientation of martensite variants. In the model, the surface energy change only affects the forward and reverse transformation while the reorientation process is not affected. The constitutive model proposed is found acceptable since the theoretical results are close to experimental data.

*Acknowledgements*—Support from the National Natural Science Foundation of China under NNSFC grants #19672026 and #19891180 and from the State Education Commission of China under the grant #9400365 is gratefully acknowledged. Japan Society for the Promotion of Science (JSPS ID No. S-97341) is acknowledged for support to KCH. The authors also thank the technical assistance from Z. J. Zhao, G. Xu, T. Xu and X. Y. Zhang in early stages of the work.

## REFERENCES

- Otsuka, K. and Shimizu, K., *Trans. JIM*, 1974, **15**, 201.
- Wechsler, M.S., Lieberman, D.S. and Read, T.A., *Trans. AIME*, 1953, **197**, 1503.
- Waman, C. M. 1964. in *Introduction to the Crystallography of Martensite Transformation*. Macmillan, New York.
- Bowles, J.S. and Mackenzie, J.K., *Acta metall.*, 1954, **2**, 129.
- Delaey, L., Krishnan, R.V., Tas, H. and Warlimont, H., *J. Mater. Sci.*, 1974, **9**, 1521.
- Christian, J.W., *Metall. Trans. A*, 1982, **13A**, 509.
- James, R.D.J., *Mech. Phys. Solids*, 1986, **34**, 359.
- Ball, J.M. and James, R.D., *Arch. Rat. Mech. Anal.*, 1987, **100**, 13.
- Bhattacharya, K., *Acta metall.*, 1991, **39**, 2431.
- Abeyaratne, R. and Knowles, J.K., *J. Mech. Phys. Solids*, 1993, **41**, 541.
- Abeyaratne, R., Chu, C. and James, R.D., *ASME Appl. Mech. Div.*, 1994, **189**, 85.
- Falk, F., *Acta metall.*, 1980, **28**, 1773.
- Patoor, E., Eberhardt, A. and Berveiller, M., *Arch. Mech.*, 1988, **40**, 775.
- Muller, I. and Xu, H., *Acta metall.*, 1991, **39**, 263.
- Chu, C. and James, R.D., *ASME Appl. Mech. Div.*, 1993, **181**, 61.
- Tanaka, K., Oberaigner, E. R. and Fischer, F. D., in *Mechanics of Phase Transformations and Shape Memory Alloys*, Vol. AMD-Vol.189/PVP-Vol.292. ASME, ed. L. C. Brinson and B. Moran, 1994, p. 151.
- Tanaka, K., Nishimura, F., Fischer, F. D. and Oberaigner, E. R., in *Proc. MECAMAT 95, J. Physique, Coll. 1, Suppl. J. Physique III*, Vol. 6, ed. C. L'excellent, E. Patoor and E. Gautier. Les Editions De Physique, Les Ulis, 1996, pp. C1–455.
- Liang, C. and Rogers, C.A., *J. Engng. Math.*, 1992, **26**, 429.
- Sun, Q.P. and Hwang, K.C., *J. Mech. Phys. Solids*, 1993, **41**, 1.
- Sun, Q.P. and Hwang, K.C., *Adv. Appl. Mech.*, 1994, **31**, 249.
- Fischer, F.D., Sun, Q.P. and Tanaka, K., *ASME Appl. Mech. Rev.*, 1996, **49**, 317.
- Fischer, F.D., Oberaigner, E.R., Tanaka, K. and Nishimura, F., *Int. J. Solids Struct.*, in press.
- Yan, W., Sun, Q. P. and Hwang, K. C., in *Proc. 3rd Asia-Pacific Symp. Advances in Engineering Plasticity and Its Application*, Japan, 1996, p. 9.
- Yan, W., Sun, Q.P. and Hwang, K.C., *Int. J. Plastic.*, 1997, **13**, 201.
- Yan, W., Sun, Q.P. and Hwang, K.C., *Sci. China*, 1998, **A28**, 275.
- Song, G. Q., Sun, Q. P. and Hwang, K. C. 1998. IUTAM Symp. Variational Domain and Free-Boundary Problems in Solid Mechanics. Paris, France. Kluwer Academic, Amsteden.
- Chen, X., Fang, D.N. and Hwang, K.C., *Smart Mater. Struct.*, 1997, **6**, 145.
- Chen, X., Fang, D.N. and Hwang, K.C., *Acta mater.*, 1997, **45**, 3181.
- Lu, Z.K. and Weng, G.J., *J. Mech. Phys. Solids*, 1997, **45**, 1905.
- Stam, G.ThM, v.d.Giessen, E. and Meijers, P., *Int. J. Solids Struct.*, 1994, **31**, 1923.
- Okamoto, K., Ichinose, S., Morii, K., Otsuka, K. and Shimizu, K., *Acta metall.*, 1986, **34**, 2065.
- Horikawa, H., Ichinose, S., Morii, K., Miyazaki, S. and Otsuka, K., *Metall. Trans. A*, 1988, **A19**, 915.
- Shield, T.W., *J. Mech. Phys. Solids*, 1995, **43**, 869.
- Sittner, P., Hara, Y. and Tokuda, M., *Metall. Mater. Trans.*, 1995, **26A**, 2923.
- Tokuda, M., Sittner, P., Takakura, M. and Ye, M., *Mater. Sci. Res. Int.*, 1995, **1**, 260.
- Lu, W., Fang, D. N. and Hwang, K. C. to be submitted.
- Dommerle, S. and Boehler, J.P., *J. Mech. Phys. Solids*, 1993, **41**, 143.
- Boehler, J.P., Demmerle, S. and Koss, S., *Exp. Mech.*, 1994, **1**.

39. Olson, G.B. and Cohen, M., *Metall. Trans.*, 1976, **7A**, 1894.
40. Mori, T. and Tanaka, K., *Acta metall.*, 1973, **21**, 571.
41. Mura, T., in *Micromechanics of Defects in Solids*. Nijhoff, Dordrecht, 1987.
42. Rice, J.R., *J. Mech. Phys. Solids*, 1971, **19**, 433–455.